Cellular/Molecular

Postsynaptic $GABA_B$ Receptor Activity Regulates Excitatory Neuronal Architecture and Spatial Memory

Miho Terunuma,[1] Raquel Revilla-Sanchez,[1] Isabel M. Quadros,[1] Qiudong Deng,[1] Tarek Z. Deeb,[1] Michael Lumb,[2] Piotr Sicinski,[3] Philip G. Haydon,[1] Menelas N. Pangalos,[4] and Stephen J. Moss[1,2]

[1]Department of Neuroscience, Tufts University School of Medicine, Boston, Massachusetts 02111, [2]Department of Neuroscience, Physiology & Pharmacology, University College London, London WC1E 6BT, United Kingdom, [3]Department of Cancer Biology, Dana-Farber Cancer Institute, Harvard Medical School, Boston, Massachusetts 02115, and [4]Innovative Medicines, AstraZeneca, Mereside, Alderley Park, Cheshire SK10 4TG, United Kingdom

Cognitive dysfunction is a common symptom in many neuropsychiatric disorders and directly correlates with poor patient outcomes. The majority of prolonged inhibitory signaling in the brain is mediated via $GABA_B$ receptors ($GABA_B$Rs), but the molecular function of these receptors in cognition is ill defined. To explore the significance of $GABA_B$Rs in neuronal activity and cognition, we created mice with enhanced postsynaptic $GABA_B$R signaling by mutating the serine 783 in receptor R2 subunit (S783A), which decreased $GABA_B$R degradation. Enhanced $GABA_B$R activity reduced the expression of immediate-early gene-encoded protein Arc/Arg3.1, effectors that are critical for long-lasting memory. Intriguingly, S783A mice exhibited increased numbers of excitatory synapses and surface AMPA receptors, effects that are consistent with decreased Arc/Arg3.1 expression. These deficits in Arc/Arg3.1 and neuronal morphology lead to a deficit in spatial memory consolidation. Collectively our results suggest a novel and unappreciated role for $GABA_B$R activity in determining excitatory neuronal architecture and spatial memory via their ability to regulate Arc/Arg3.1.

Introduction

Cognitive dysfunction is an important diagnosis of many neurological and psychiatric disorders. Spatial and contextual learning is largely dependent on the hippocampus and is mediated by persistent changes in neuronal activity and structure.

Sustained inhibitory signaling in the brain is mediated by $GABA_B$ receptors ($GABA_B$Rs), which are members of the C-class subfamily of G-protein-coupled receptors. $GABA_B$Rs are obligate heterodimers composed of two related subunits, $GABA_B$R1 and $GABA_B$R2 (Kaupmann et al., 1997; Bowery et al., 2002). The inhibitory effects of $GABA_B$Rs on neuronal activity are mediated by decreased neurotransmitter release via inhibition of N/P/Q-type Ca^{2+} channels and by postsynaptic hyperpolarization via the activation of GIRK channels by G$\beta\gamma$ dimer (Mott and Lewis, 1994; Takahashi et al., 1998; Couve et al., 2000). $GABA_B$Rs localize to both the presynaptic and postsynaptic sites of glutamatergic and GABAergic neurons. $GABA_B$Rs are predominantly localized to the perisynaptic sites of dendritic spines, where the receptors enable rapid regulation of excitatory transmission. $GABA_B$Rs are also localized to the inhibitory synapses on the dendritic shafts (Bettler and Tiao, 2006). Consistent with this, changes in the efficacy of $GABA_B$Rs are critical for the control of neuronal activity and cognitive performance (Bowery et al., 2002). $GABA_B$R antagonists enhance cognition in mammals (Mondadori et al., 1993; 1996; Brucato et al., 1996), while agonists suppress working memory (DeSousa et al., 1994).

Modulation of $GABA_B$R signaling occurs at multiple levels, including receptor assembly, trafficking, cell-surface stability, and effector coupling. A number of studies have reported the modulation of $GABA_B$Rs by signal transduction pathways that activate protein kinases and phosphatases (Terunuma et al., 2010a). Protein kinase A decreases receptor rundown by phosphorylation of serine 892 in the cytoplasmic tail of the $GABA_B$R2 subunit, thereby enhancing $GABA_B$R activation of GIRKs (Couve et al., 2002). In addition, the $GABA_B$R2 subunit is phosphorylated on S783 by 5′ AMP-dependent protein kinase (AMPK), which also enhances receptor coupling to GIRKs (Kuramoto et al., 2007). Phosphorylation of S783 is modulated via the activity of NMDA receptors (NMDARs). Transient activation of NMDARs leads to enhanced phosphorylation, whereas prolonged NMDAR activation results in dephosphorylation of $GABA_B$Rs by protein phosphatase 2A (PP2A), which in turn selectively targets the receptors for lysozomal degradation. Thus phosphorylation of S783 is likely to play a key role in

Received Aug. 3, 2013; revised Nov. 25, 2013; accepted Nov. 26, 2013.

Author contributions: M.T. and S.J.M. designed research; M.T., R.R.-S., I.M.Q., Q.D., T.Z.D., and M.L. performed research; M.T., P.S., P.G.H., M.N.P., and S.J.M. contributed unpublished reagents/analytic tools; M.T., R.R.-S., I.M.Q., Q.D., T.Z.D., and P.G.H. analyzed data; M.T., T.Z.D., and S.J.M. wrote the paper.

M.T. was a recipient of a National Scientist Development Grant (09SDG2260557) from the American Heart Association. S.J.M. is supported by NIH–National Institute of Neurological Disorders and Stroke Grants NS051195, NS056359, NS081735, and MH097446; and by Citizens United for Research in Epilepsy (PV0178) and the Simons Foundation (PV0138). We thank to the members of the Moss Laboratory for discussions during the course of this study and Dr. M. Ericsson for help and advice.

S.J.M. serves as a consultant for Sage Therapeutics and Astra Zeneca, relationships that are regulated by Tufts University and do not impact on this study.

Correspondence should be addressed to either of the following: Miho Terunuma, DDS, PhD, Department of Cell Physiology and Pharmacology, College of Medicine, Biological Sciences and Psychology, University of Leicester, University Road, Leicester LE1 9HN, United Kingdom. E-mail: mt304@le.ac.uk; or Stephen Moss, PhD, Astra Zeneca Laboratory of Translational Neuroscience, Department of Neuroscience, Tufts University School of Medicine, 136 Harrison Avenue, Boston, MA 02111. E-mail: Stephen.Moss@tufts.edu.

M. Terunuma's present address: Department of Cell Physiology and Pharmacology, College of Medicine, Biological Sciences and Psychology, University of Leicester, University Road, Leicester LE1 9HN, United Kingdom.

DOI:10.1523/JNEUROSCI.3320-13.2013

 0270-6474/14/330804-13$15.00/0

regulating the efficacy of $GABA_BR$ activity and signaling, but its influence on cognition remains to be evaluated (Terunuma et al., 2010b).

To test the role that phospho-dependent modulation of $GABA_BRs$ play in synaptic transmission and memory formation, we generated a knock-in mouse in which S783 was mutated to alanine (S783A). We found that $GABA_BR$ degradation was necessary for hippocampal-dependent spatial memory by regulating protein important for memory formation. Mutation of S783 increased the expression of postsynaptic $GABA_BRs$ by blocking receptor degradation, which decreased levels of Arc/Arg3.1, a protein necessary for memory consolidation (Plath et al., 2006). In contrast, we found an increase in the number of excitatory synapses and elevated surface AMPA receptors (AMPARs), which correlates with reduced Arc/Arg3.1. Collectively these experiments demonstrate a critical role for $GABA_BR$ modulation in regulating neuronal architecture and cognition.

Materials and Methods

Generation of mice lacking phosphorylation site in $GABA_BR2$ subunit

The construct was generated by PCR from C57BL/6 genomic DNA. Two overlapping PCR products were generated. The first contained a 3.4 kb left arm followed by exon 16. The second contained exon 16 followed by a 2.2 kb right arm. These were cloned (5′–3′) into the NotI/EcoRI sites of pBluescriptIIKS$^+$ (Stratagene). Exon 16 contains a unique BstBI site upstream of serine 783.

The vector had been modified in the following ways. First, the KpnI site was replaced by SpeI site and then the SalI polylinker site removed. In addition, to stabilize the inserts and improve cloning efficiency, the vector was modified for low copy number by insertion of the *rop* gene from pBR322 into the NgoMIV site in the plasmid backbone.

Site-directed mutagenesis (Stratagene) was used to mutate serine 783 in construct 2 to alanine and to create a SalI site 200 bp downstream of exon 16. The full-length construct was created by cloning the BstBI/EcoRI fragment of construct 2 into construct 1. A *loxP*-flanked neomycin-positive selection cassette was cloned into the SalI site in reverse orientation with respect to exon 16. A thymidine kinase-negative selection cassette was inserted at the 3′ end of the full-length construct in reverse orientation between the SpeI and ClaI sites of pBluescript.

The construct was linearized with NotI and electroporated into 129Sv/Pas ES cells. Positive clones were identified by PCR and confirmed by Southern blot using an outer probe. Two positive ES clones were injected into C57BL/6J blastocysts and the chimera were crossed to C57BL/6J mice. These mice were crossed to CMV-Cre mice to remove the neo cassette from the germ line. After confirmation of neo excision by PCR, heterozygous mice were bred to produce homozygotes. All procedures have been approved by Tufts University's Institutional Animal Care of Use Committee.

Western blot

Standard Western blot protocol was used as previously described (Terunuma et al., 2004). Protein samples were subjected to SDS-PAGE gels and transferred to supported nitrocellulose membrane. Membranes were blocked with blocking buffer [5% bovine serum albumin (BSA) in TBST]. Membranes were probed with primary antibodies against $GABA_BRs$ [$GABA_BR1$, University of California Davis/National Institutes of Health (NIH) NeuroMab, N94A/49; $GABA_BR2$, University of California Davis/NIH NeuroMab, N81/37], phospho-S783 (Terunuma et al., 2010b), tubulin (Sigma-Aldrich), GAPDH, ERK2 (Santa Cruz Biotechnology), synaptophysin, phospho-ERK, phosphocofilin, cofilin (Cell Signaling Technology), Arc/Arg3.1, synapsin I (Synaptic Systems), and PSD-95 (postsynaptic density-95; Affinity BioReagents). Membranes were then probed with HRP-conjugated secondary antibodies and visualized by ECL. Blots were then quantified using the CCD-based FujiFilm LAS 3000 system.

Immunoprecipitation

Tissue homogenates from adult mice hippocampus were prepared as previously described (Terunuma et al., 2004). For immunoprecipitation, 200 μg of homogenates were incubated for 2 h with 1 μg of mouse anti-$GABA_BR1$, anti-$GABA_BR2$, or purified mouse IgG (Santa Cruz Biotechnology). Mouse immunoprecipitation matrix (ImmunoCruz IP/WB Optima, Santa Cruz Biotechnology) was added and the mixture was incubated at 4°C for another 2 h. The beads were spun down at 12,000 × *g* for 15 s and then washed three times with lyses buffer containing 300 mM NaCl. The fourth and fifth wash was performed with normal lyses buffer. The beads were eluted in 2× sample loading buffer following the same procedure as for immunoblotting except using mouse-ExtraCruz-HRP (Santa Cruz Biotechnology) as a secondary antibody.

Immunohistochemistry

Eight-week-old male mice were deeply anesthetized and intracardially perfused with saline solution followed by 4% of paraformaldehyde. Brains were removed, postfixed overnight, and cryoprotected in 30% sucrose. Free-floating sections were then cut at 40 μm in a freezing microtome and kept at −20°C in cryoprotective solution (30% sucrose, 30% ethylenglycol, 1% polyvinylpyrrolidone in PBS) until processing. For immunostaining, sections were washed in PBS and incubated for 2 h in blocking solution (2% normal horse serum, 0.5% BSA, and 0.5% Triton X-100 in PBS) followed by incubation in blocking solution containing the following primary antibodies: guinea pig anti-$GABA_BR2$, rabbit anti-PSD-95, and mouse anti-synaptophysin (all from Millipore), for 72 h at 4°C. After rinsing in PBS, sections were incubated in blocking solution containing secondary antibodies (anti-rabbit-Rhodamine Red-X, anti-guinea pig-fluorescein, and anti-mouse-Cy5) for 2 h at room temperature, then rinsed in PBS and mounted in slides. Sections were visualized in a Nikon confocal microscope and the intensity was analyzed using MetaMorph software (Universal Imaging).

Surface labeling of hippocampal slices and cultured neurons

Hippocampal slices were incubated in ACSF at 32°C for at least 1.5 h recovery before experimentation. Slices were then incubated for 30 min with 1 mg/ml N-hydroxysuccinimide-SS-biotin and lysed as described previously (Terunuma et al., 2008, 2010b).

Field potential recording

Slices from 6–12-week-old S783A and WT littermates were prepared as described previously (Deng et al., 2011). Slices were transferred in a recording chamber mounted to an upright microscope (BX51WI, Olympus) and continuously superfused (1.5–2 ml/min) with ACSF saturated with 95% O_2/5% CO_2 at 32–35°C helped by an automatic temperature controller (Warner Instruments). CA3 to CA1 connections were cut and field potentials from the CA1 stratum radiatum were recorded with an extracellular glass pipette (1–2 MΩ) filled with ACSF. Schaffer collaterals were stimulated at 0.033 Hz with 100 μs pulses though a concentric stimulation electrode (FHC) placed in the stratum radiatum near the CA1 border to stimulate the Schaffer collateral. Stimulation intensities were chosen to produce a field EPSP with amplitude that was 40–50% of those obtained with maximal stimulation. LTP was electrically induced by using two or five theta-burst stimulations at 0.033 Hz. One theta burst consisted of 40 ms duration 100 Hz trains, repeated four times at 200 ms intervals.

Electrophysiology in cultured hippocampal neurons

Mouse hippocampal neurons were dissected at embryonic day 17 and plated onto glass coverslips at a density of 100,000 per 35 mm dish. Neurons were incubated in Neurobasal A media for 14–18 d before recordings. Recordings were performed in bath saline containing the following: 140 mM NaCl, 4.7 mM KCl, 2.5 mM $CaCl_2$, 1.2 mM $MgCl_2$, 10 mM HEPES, 11 mM glucose, pH 7.4 by NaOH. AP5 (50 μM), DNQX (20 μM), bicuculline (50 μM), and TTX (500 nM) were added to the bath saline to block NMDARs, AMPARs, and $GABA_ARs$ and Na_V channels, respectively. Baclofen (10 μM) was used for $GABA_BR$ activation. The patch pipette contained the following: 134 mM K-gluconate, 6 mM KCl, 0.1 mM $CaCl_2$, 2 mM $MgCl_2$, 1.1 mM EGTA, 10 mM HEPES, 2 mM ATP, 1 mM GTP, pH 7.4 by KOH. Recordings were performed at 34°C using an

Axopatch 200B amplifier. Current density values were equivalent to the averaged current amplitudes of three consecutive baclofen pulses spaced 1 min apart, divided by the whole-cell capacitance. Current recordings were performed at −50 mV with a calculated E_K value of −90 mV, the resulting driving force of ~+40 mV caused outward baclofen-activated K^+ currents.

Electron microscopy

Animals were perfused intracardially with 2.5% glutaraldehyde, 2% paraformaldehyde. Tissues were postfixed with 1% osmium tetroxide/1.5% potassium ferrocyanide and embedded in TAAB Epon. Ultrathin sections were stained with lead citrate and examined in a JEOL 1200EX or a Tecnai G^2 Spirit BioTWIN transmission electron microscope. Images were recorded with an Advanced Microscopy Techniques 2000-pixel CCD camera. PSD length was measured using ImageJ software.

Behavioral analyses

All mice used were adult 2–3-month-old male S783A mice and control littermates obtained by crossing heterozygote mice. Experiments were performed at the Center for Neuroscience Research Animal Behavior Core, Tufts University. Animals were maintained in a controlled environment under a reversed 12 h light/dark cycle with lights off at 7 A.M. (lights on at 7 P.M.). All testing occurred during the dark phase, when mice are most active, as described previously (Tretter et al., 2009).

Fear-conditioning test. Fear conditioning was performed in Coulboum test cages (Model H10-11R-TC) equipped with grid shock floors. On the training day, each mouse was placed in the test cage for 5 min. After 3 min of exploration, animals received two pairings of a 30 s tone (80 dB) with a foot shock (0.5 mA, 2 s), with 30 s interval. The foot shock was presented overlapping with the final 2 s of the tone. Twenty-four hours later, each animal was placed back in the original test chamber for 5 min without any stimulus (no shock, no tone) to assess context-associated fear conditioning. A plastic container (17 cm height × 19 cm width × 28 cm length) with bedding on the floor and black-and-white patterns on the walls was placed within the test chamber, and mice were placed into the plastic container for a 6 min cued fear test. After 3 min of no stimulus (pretone), mice were subjected to three evenly spaced 30 s tones (80 dB, no shock presented, identical to ones experienced during the training session). Freezing behavior was used as index of fear memory, and was automatically detected with Actimetrics Freeze Frame 2.10 software, a video-based system. Percentage of time each animal spent freezing was measured in all conditions (training, context, and tone tests).

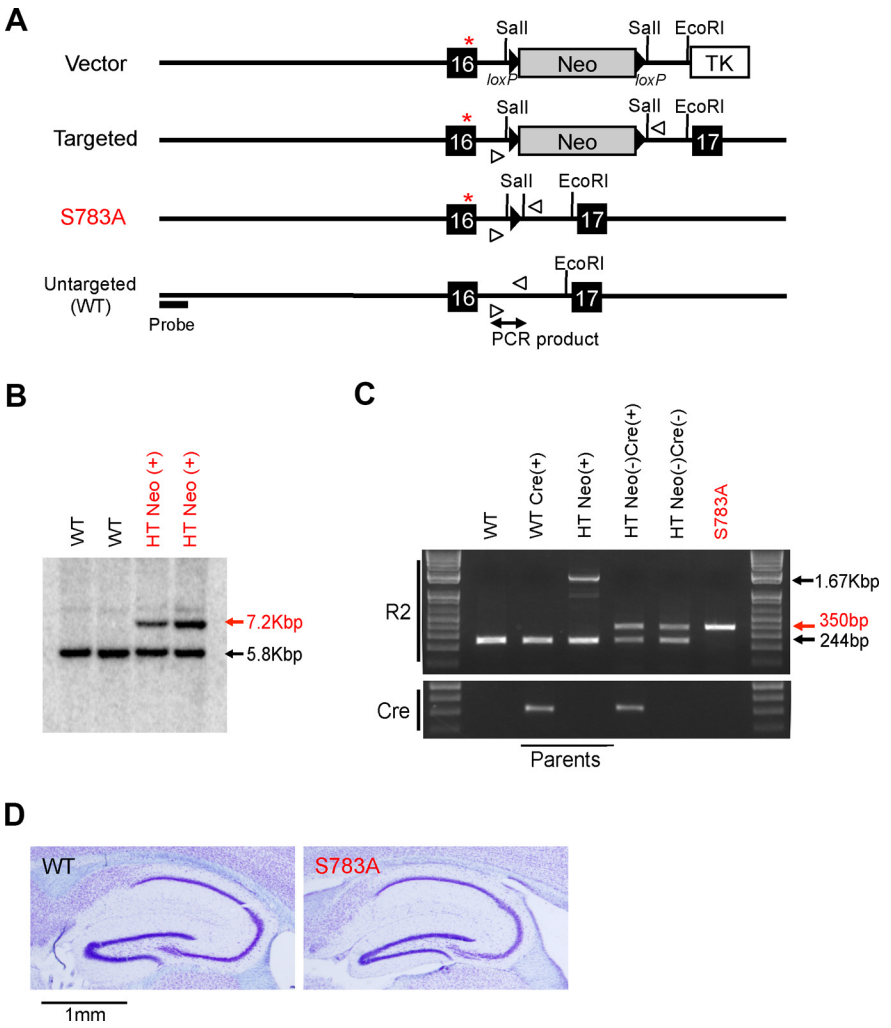

Figure 1. Generation of mice with mutated S783 phosphorylation site in $GABA_BR2$ subunit. ***A***, Schematic representations of the structures of targeting vector, targeted and Neo-targeted (S783A) $GABA_BR$ allele, and WT (Untargeted) allele. *TK*, thymidine kinase gene; *Neo*, neomycin resistance gene with *loxP* sequence at both sides. The probe is depicted as solid bar. ***B***, Southern blot from mice tail samples. Two positive clones (7.2 kbp) were selected. ***C***, PCR analysis of indicated samples. PCR for $GABA_BR2$ (top) and Cre (bottom). ***D***, Nissl-stained representative sagittal sections from WT and S783A mice. No significant changes were observed in hippocampal gross anatomy. Scale bar, 1 mm.

Novel- object recognition. The novel-object recognition task is based on the innate tendency of rodents to differentially explore novel objects over familiar ones. The test was performed as previously described (Ennaceur and Delacour, 1988). Mice were placed into a Plexiglas rectangular cage (22 cm height × 44 cm length × 22 cm width) for 10 min. In the training trial (familiarization phase), the animals were presented with a pair of identical objects (~15 cm height × 4 cm width × 4 cm length) that had been placed in the opposite corners for 10 min. The exploration of the objects is considered when a mouse shows any investigative behavior (head orientation or sniffing occurring), or entering an area within 1 cm around the object. In the testing trial (testing phase, performed 24 h later), one of the familiar objects was changed for another one (novel object), and the animals were left in the cage for 10 min. The exploration time for the familiar or the novel object during the test phase was recorded. Control WT mice are expected to spend more time exploring the novel object than the familiar object, indicating learning and memory retrieval.

Spatial object recognition. Mice were habituated to a Plexiglas rectangular cage (22 cm height × 44 cm length × 22 cm width) for 10 min. On the next day, mice were returned to the cage in which two identical objects (~15 cm height × 4 cm width × 4 cm length) had been placed in the opposite corners. Mice were allowed to explore for 10 min, and the time of interaction with the objects was measured. Interaction consisted of sniffing, touching, or entering an area within 1 cm around the object, while orienting toward it. On next day (24 h after training), one of the objects was moved (displaced object) while the other one was left in the same spatial position (nondisplaced). Time exploring each object was recorded. Control, WT mice are expected to spend more time exploring the displaced object than the familiar, nondisplaced object, indicating spatial learning and memory retrieval.

Barnes maze task. Barnes circular maze was an acrylic disc 122 cm in diameter, one-quarter inch thick that was painted with white epoxy paint. Forty holes, 5 cm diameter, were located 5 cm from the perimeter,

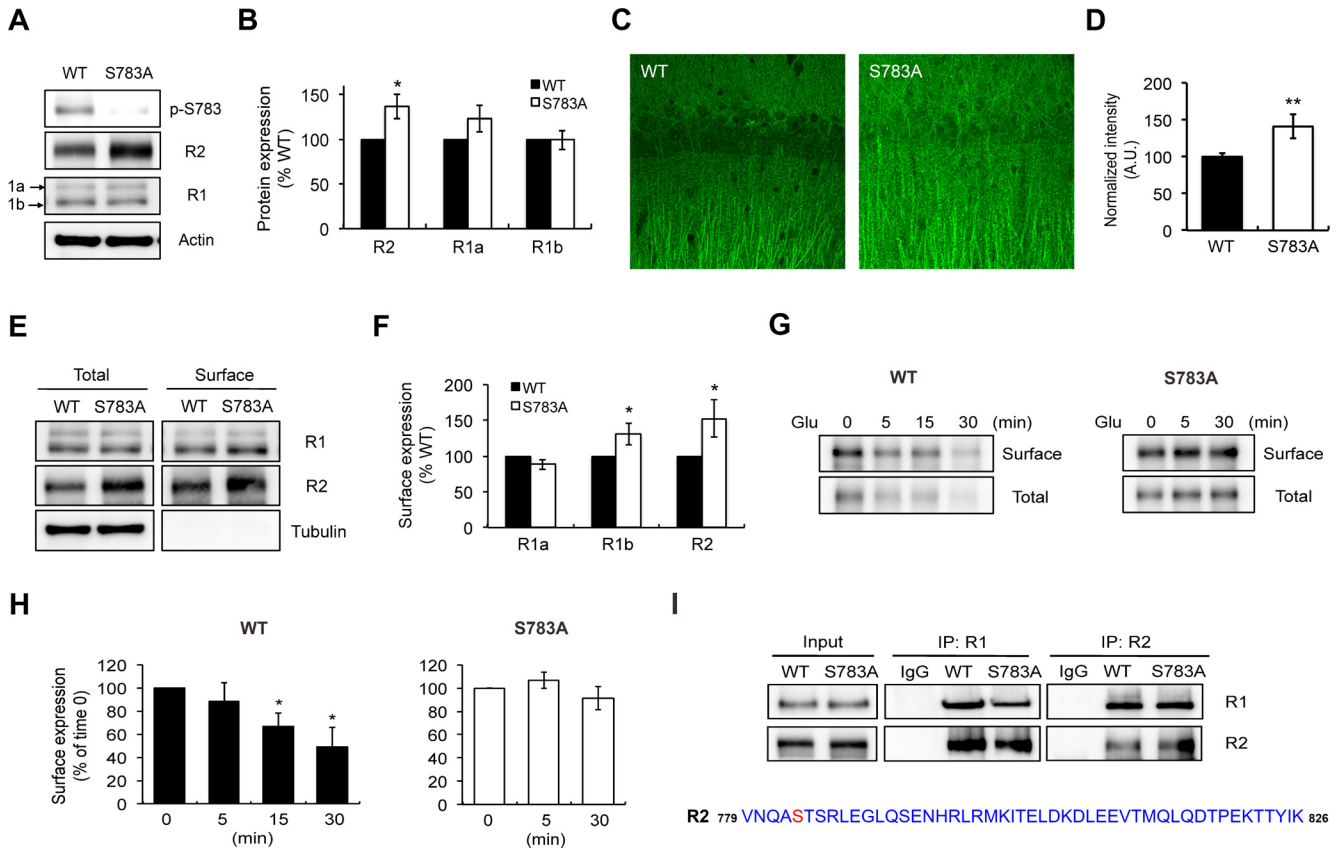

Figure 2. Analysis of $GABA_BR$ expression in S783A mice. ***A***, Western blot analysis of hippocampus dissected from WT and S783A mice. Immunoblots were probed with antibodies using phosphorylation site-specific antibody against S783 (p-S783), or antibodies recognizing total $GABA_BR2$ (R2) and $GABA_BR1$ (R1) subunits, or actin. ***B***, Quantification of $GABA_BR2$ and $GABA_BR1$ subunits in hippocampi of adult S783A mice. Integrated intensities were calculated by densitometry measurements of immunoblots in ImageJ, and were normalized to averages of actin levels. Data are shown as a change relative to WT and represent mean ± SEM. $n = 9$, $^*p < 0.05$; Student's *t* test. ***C***, Representative confocal images of hippocampal CA1 region immunostained for $GABA_BR2$ subunit in WT and S783A mice. ***D***, Normalized quantification of $GABA_BR2$ subunit expression of CA1 region of the hippocampus in WT and S783A mice. Shown are mean ± SEM from five independent experiments. $^{**}p < 0.01$; Student's *t* test. ***E***, Increased surface expression of $GABA_BRs$ in S783A mice. Hippocampal slices prepared from WT and S783A mice were used for steady-stated biotinylation of surface $GABA_BRs$. Total expressions are shown to the left, and the biotinylated surface $GABA_BR1$ and $GABA_BR2$ subunits are shown to the right. Tubulin was used as a control. ***F***, Quantification of surface $GABA_BR$ levels in WT and S783A mice. Data are normalized to WT and represented mean ± SEM. $n = 9–10$, $^*p < 0.05$; Student's *t* test. ***G***, Reduced steady-state surface expression of $GABA_BR2$ subunit by glutamate (20 μM) activated in WT hippocampal slices but not in S783A slices. ***H***, Normalized quantification of $GABA_BR2$ subunit expression in WT and S783A hippocampal slices. Shown are mean ± SEM from five independent experiments. $^*p < 0.05$; Student's *t* test. ***I***, Coimmunoprecipitation of $GABA_BRs$ from adult mouse hippocampal extracts. Crude hippocampal lysates were immunoprecipitated with antibodies that recognize $GABA_BR1$ and $GABA_BR2$ subunits. Precipitated materials were then immunoblotted with the indicated antibodies to detect $GABA_BR$ heterodimer. Total lysates (Input) were also analyzed. Sequence of coiled-coil domain in $GABA_BR2$ subunit is shown in blue. Serine 783 is marked in red.

and a black escape tunnel was placed under one hole. Distal cues were placed around the room. On the first day (pretraining), mice were trained to enter the escape box (target) by (1) placement into the escape box for 2 min and (2) guidance to the escape box, where they remained for 2 min. The following day, mice were briefly placed in the center of the maze under a removable chamber and given 3 min to locate the escape box. At the beginning of each session, mice were placed in the middle of the maze in a 10-cm-high cylindrical black start chamber, and a buzzer (80 dB) was sounded. After 10 s of a buzzer, the chamber was lifted and the mice were free to explore the maze. The primary and total number of errors (incorrect hole pokes), primary and total latency to locate and enter the escape box, and the navigation patterns were recorded. Mice that failed to enter the escape box within 3 min were guided to the box and remained for 2 min before returning to their home cage. Mice received 2 trials/d, separated by 15 min, for 4 d. After each trial, the entire maze was cleaned with ethanol.

One day after the acquisition phase, subjects performed a probe trial for 90 s to check the retention memory on days 5 and 12. Mice were allowed to explore the maze and the following parameters were evaluated on days 5 and 12 with the target hole closed: primary latency, primary error, primary path length, and visits to the target hole and the adjacent holes. Mice were not trained between days 5 and 12.

Home cage activity. Animals were placed individually into standard plastic home cages with food and water available *ad libitum*. Motor activity was monitored with the SmartFrame Cage Rack System (Kinder Scientific). This system consists of 24 PC-interfaced horizontal photobeam frames. The frame (containing 12 photocells; 9 cm length × 4 cm width) surrounds one home cage environment and continuously tracts the animal's movement. Using MotorMonitor software (Kinder Scientific), data were collected in the form of photobeam breaks as an indication of activity within different predetermined "zones" in the home cage. The data were collected and analyzed every 10 min for 2 h.

Elevated plus maze test. Animals were placed individually into the center of a fully automated elevated plus maze (Kinder Scientific) consisting of two open arms (38 cm length × 5 cm width) and two closed arms (38 cm length × 5 cm width × 15 cm height), with a central intersection (5 cm × 5 cm) elevated 75 cm above the floor. Movement through the maze was detected by 48 equally spaced photocells. The test lasted 5 min. All data were automatically collected and quantified using MotorMonitor software (Kinder Scientific). The data were subsequently reduced to the following parameters for each arm and the center: basic movements (beam breaks), distance traveled (in centimeters), time spent (in seconds), number of full entries, number of pokes unto, number of head dips over the side of the open arm.

Results

Generation of $GABA_BR2$ S783A knock-in mice

We generated mutant mice in which S783 was substituted with an alanine residue using homologous recombination to directly examine the physiological role of $GABA_BR$ phosphorylation and dephosphorylation (Fig. 1*A*). Successful gene targeting was confirmed by Southern blot and PCR analyses (Fig. 1*B*,*C*). S783A mice were born according to Mendelian genetics and appeared healthy. Histological analysis by Nissl-staining of hippocampal sections from S783A mice did not show any gross abnormalities in cytoarchitecture compared with WT (Fig. 1*D*). We then confirmed the absence of phosphorylated-S783 (pS783) in S783A mice by Western blot analysis using an anti-pS783 antibody that specifically recognizes the $GABA_BR2$ subunit only when phosphorylated at S783 (Fig. 2*A*; Kuramoto et al., 2007; Terunuma et al., 2010a). Interestingly, the total expression of $GABA_BR2$ subunit was significantly increased in S783A mice ($p < 0.05$). At hippocampal CA3-to-CA1 synapses, $GABA_BRs$ containing R1a subunits are components of presynaptic receptors that inhibit glutamate release, whereas those containing R1b largely mediate postsynaptic inhibition. In contrast, $GABA_BRs$, which control GABA release, contain both R1a and R1b subunits (Vigot et al., 2006). We therefore examined the expression of $GABA_BR1a$ and $GABA_BR1b$ subunits and found no differences between the genotypes in the hippocampus ($p > 0.05$; Fig. 2*A*,*B*). Immunohistochemical staining of brain sections using anti-$GABA_BR2$ antibody confirmed that the $GABA_BR2$ subunit intensity was increased in the CA1 hippocampal region of S783A mice ($p < 0.01$; Fig. 2*C*,*D*).

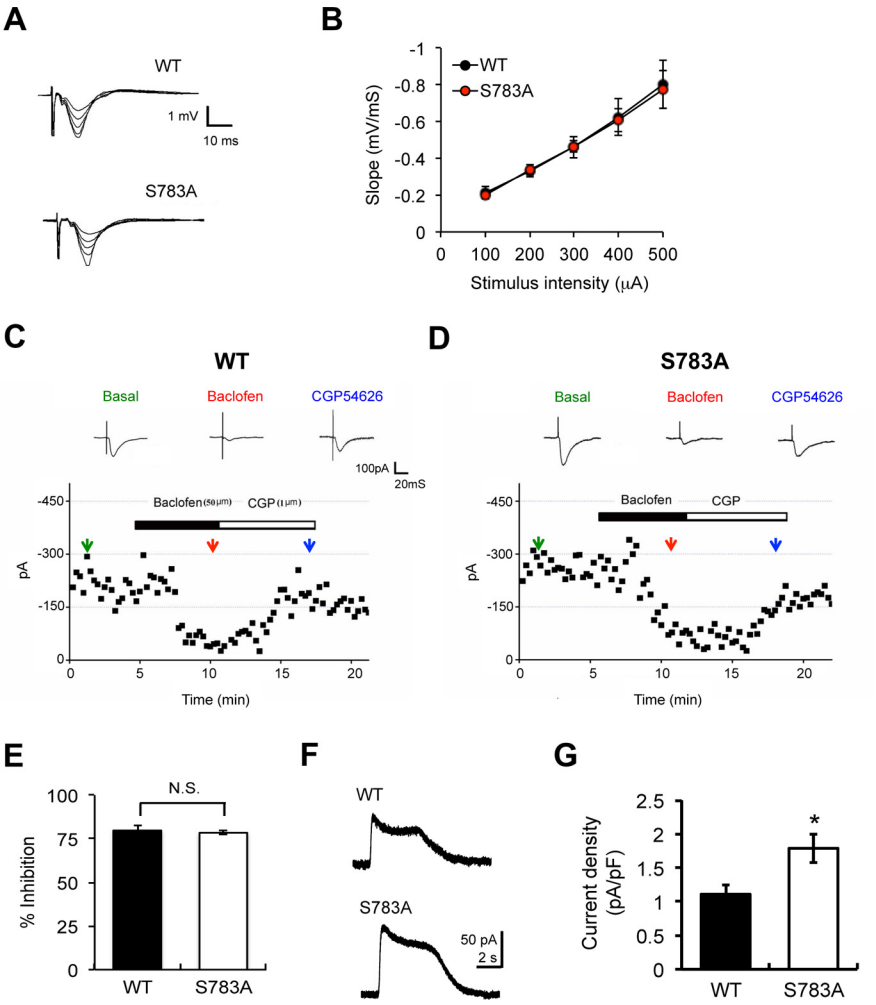

Figure 3. Enhanced postsynaptic $GABA_BR$ activity in S783A mice. ***A–B***, Normal basal excitatory synaptic transmission measured in S783A mice. ***A***, Representative traces from WT and S783A animals show input– output measurements with increasing stimulus intensities. Responses were measured in CA1 of mouse hippocampus. ***B***, Average fEPSP slope plotted against various stimulus intensities are shown. Data are shown as a change relative to WT and represent mean ± SEM ($n = 8$, $p = 0.8256$, 2-way ANOVA). ***C–E***, Peak amplitudes and representative traces from WT mice (***C***) and S783A mice (***D***), and summary histogram of EPSC in hippocampus CA1 region (***E***). Baclofen suppresses the amplitude of EPSCs in both WT mice (78.44 ± 2.63%) and S783A mice (79.98 ± 1.02%). Data are mean ± SEM. Two-tailed *t* test, $p = 0.61$. ***F***, ***G***, The S783A mice exhibit higher current densities. ***F***, Recordings of baclofen-activated (10 μM) currents were obtained from WT and S783A hippocampal neurons at a holding potential of −50 mV. Neurons were bathed in saline containing AP5, DNQX, TTX, and bicuculline. ***G***, Data are shown as a change relative to WT and represent mean ± SEM ($n = 5$, $^*p < 0.05$, unpaired *t* test).

Phosphorylation of S783 increases the abundance of $GABA_BRs$ at the plasma membrane and decreases rundown of the $GABA_BR$-activated GIRK currents (Kuramoto et al., 2007). On the other hand, dephosphorylation of S783 by PP2A promotes lysozomal degradation of $GABA_BRs$ (Terunuma et al., 2010b). Since studies *in vitro* have revealed that mutation of S783A prevents the rundown of $GABA_BR$-mediated currents and increases receptor stability (Kuramoto et al., 2007; Vargas et al., 2008; Terunuma et al., 2010b), we first examined the steady-state levels of $GABA_BRs$ on the plasma membrane of hippocampal slices (Terunuma et al., 2008). Biotinylation assays revealed that mutation of S783 to an alanine increased the cell-surface levels of $GABA_BR1b$ and $GABA_BR2$ subunits ($p < 0.05$), which are mostly postsynaptic, but not of the presynaptic $GABA_BR1a$ subunit (Fig. 2*E*,*F*). We then examined whether the S783A mutation impacted glutamate-dependent downregulation of $GABA_BRs$ (Vargas et al., 2008; Terunuma et al., 2010b). Consistent with published studies, treatment of slices from WT mice induced significant degradation of surface R2 subunits, an effect that was completely abrogated in S783A mice (Fig. 2*G*,*H*; Terunuma et al., 2010b). These data suggested that S783A mutation *in vivo* is resistant from degradation and, therefore, $GABA_BRs$ are expressed significantly higher in S783A mice.

As S783 is found at the N terminus of the coiled-coil domain (Kuramoto et al., 2007), we examined whether S783A mutant $GABA_BR2$ subunits are capable of dimerizing with $GABA_BR1$ (Fig. 2*I*). As measured using coimmunoprecipitation followed by immunoblotting, mutation of S783 did not appear to compromise the formation of R1/R2 subunit dimers (Fig. 2*I*). Together the S783A mutation enhanced the cell-surface expression levels of $GABA_BRs$ containing R1a/R2 subunits by prevented glutamate-induced receptor degradation.

Enhanced postsynaptic $GABA_BR$ activity in S783A mice

Since S783A mice have elevated cell-surface accumulation of $GABA_BRs$, we examined whether the mutation of this residue

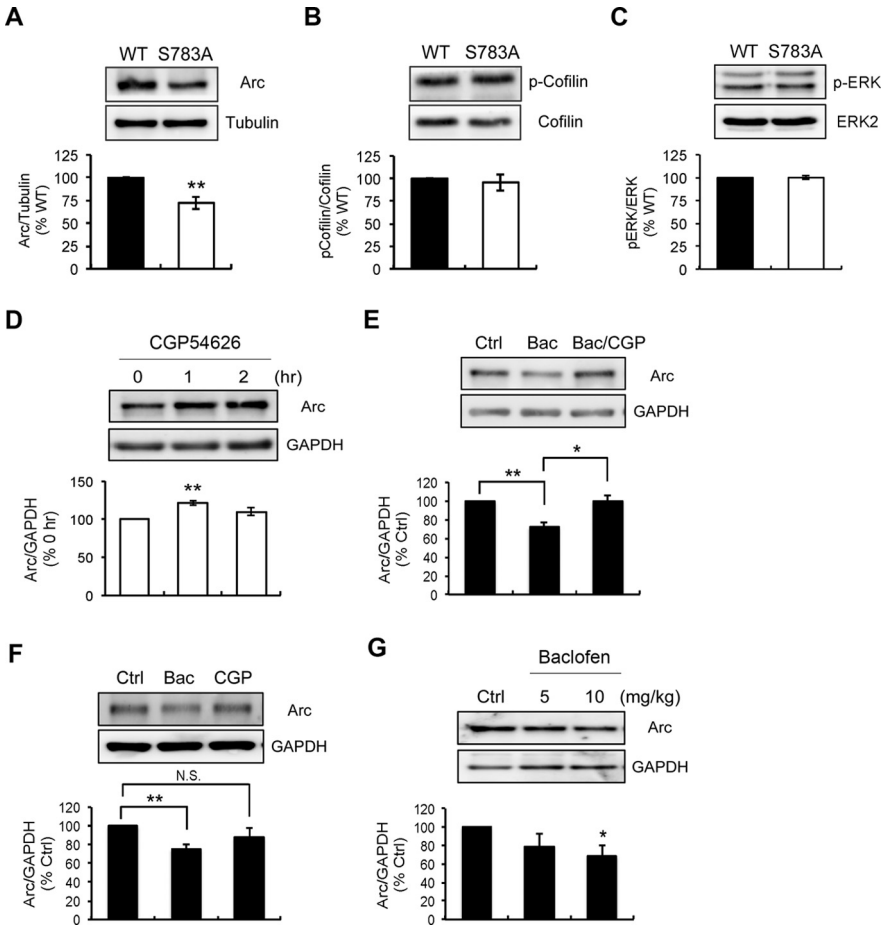

Figure 4. Expression of proteins important for memory formation in S783A mice. ***A–C***, Measurement of proteins important for memory consolidation. S783A decreased Arc/Arg3.1 (***A***), but not p-cofilin (***B***) and p-ERK (p42/p44) of ERK (***C***) levels. Data are shown as a change relative to WT and represent mean ± SEM. $n = 6$, $^*p < 0.05$, $^{**}p < 0.01$, unpaired t test. ***D***, Prolonged CGP54626 (10 μM) increase Arc/Arg3.1 expression in S783A mice. Data are shown as a change relative to control (0 h) and represent mean ± SEM. $n = 4$, $^{**}p < 0.01$, one-way ANOVA. ***E***, ***F***, Baclofen treatment decreases Arc/Arg3.1 expression in WT mice. Hippocampal slices from WT mice were stimulated with baclofen or together with CGP54626 (***E***). The effect to CGP54626 alone was shown in ***F***. Data are shown as a change relative to control (Ctrl) and represent mean ± SEM. $n = 4$, $^*p < 0.05$, $^{**}p < 0.01$, Student's t test. ***G***, Intraperitoneal injection of baclofen reduces Arc/Arg3.1 expression in WT mice. Baclofen (5 and 10 mg/kg) or saline vehicle were given for 60 min. Animals were immediately decapitated and the expression of Arc/Arg3.1 was quantified by Western blotting. Data are normalized to saline (Ctrl) and represented mean ± SEM. $n = 4$, $^*p < 0.05$; one-way ANOVA.

modifies $GABA_B$R function in hippocampal slices. We first examined basal synaptic transmission in CA1. We found that the input–output coupling during stimulation of the Schaffer collaterals were identical in WT and S783A mice, indicating similar levels of basal synaptic strength (Fig. 3*A*,*B*). To examine whether presynaptic $GABA_B$R function is altered in S783A mice, we stimulated Schaffer collateral fibers and measured the amplitudes of EPSCs in CA1 pyramidal neurons, which can be reduced by activation of presynaptic $GABA_B$Rs (Schuler et al., 2001). Baclofen reduced the EPSC amplitude in both WT and S783A mice to similar extents ($p = 0.61$), suggesting that the $GABA_B$R function on Schaffer collateral terminals was comparable between strains (Fig. 3*C–E*). We did not observe differences in basal-evoked EPSCs between WT and S783A mice as well (WT: -263 ± 31 pA; S783A: -310 ± 31 pA, $p = 0.3889$). Together these data suggested that S783 phosphorylation does not significantly impact presynaptic $GABA_B$R function at glutamatergic synapses.

Next, using cultured hippocampal neurons, we examined whether the function of postsynaptic $GABA_B$Rs was altered in S783A mice. At 14–18 DIV, we measured $GABA_B$R activation of GIRK channels using baclofen (Kuramoto et al., 2007; Terunuma et al., 2010b). In agreement with our biochemical analysis, S783A mice exhibited significantly higher current density values compared with WT ($p = 0.0047$; Fig. 3*F*,*G*). Therefore, consistent with our biochemical experiments, mutation of S783A leads to a selective increase in the expression levels and activity of postsynaptic $GABA_B$Rs.

Arc/Arg3.1 expression is regulated by $GABA_B$R activity

Changes in the efficacy of $GABA_B$R activity and signaling are critical for the control of neural activity and cognitive performance (Bowery et al., 2002). Recent studies have suggested that the immediate-early gene-encoded protein Arc/Arg3.1 is broadly responsive to neuronal activation by physiological stimuli and is an essential requirement for memory consolidation (Link et al., 1995; Guzowski et al., 2000). Arc/Arg3.1 is upregulated by neural activity, such as activation of NMDARs and Group 1 metabotropic glutamate receptors (Shepherd et al., 2006; Bloomer et al., 2008; Waung et al., 2008). Because $GABA_B$Rs regulate neural activity, we analyzed the expression of Arc/Arg3.1 in S783A mice. We found significant and robust reductions in the expression of Arc/Arg3.1 in S783A hippocampus (Fig. 4*A*). In contrast, the phosphorylation of the actin-binding protein cofilin, which regulates the dynamics of the actin cytoskeleton and modifies the size of dendritic spines (Gu et al., 2010; Rust et al., 2010), was unchanged in S783A mice (Fig. 4*B*). We also found no difference in ERK phosphorylation (Fig. 4*C*), which is involved in several protein syntheses important for long-term memory (Satoh et al., 2007). Collectively these results suggest a selective effect of enhanced $GABA_B$R signaling on Arc/Arg3.1 expression.

To determine whether modified Arc/Arg3.1 expression in S783A mice result from elevated levels of $GABA_B$R activity, we treated S783A hippocampal slices with the $GABA_B$R antagonist CGP54626 (10 μM). Arc/Arg3.1 levels were increased after 1 h treatment with CGP54626 (Fig. 4*D*). To further evaluate the role of $GABA_B$Rs in mediating Arc/Arg3.1 expression, hippocampal slices from WT mice were treated with baclofen, which decreased Arc/Arg3.1 expression, an effect prevented by the $GABA_B$R antagonist CGP54646 (Fig. 4*E*,*F*).

Finally, we performed systemic injection of baclofen (10 mg/kg, i.p.) in WT mice and measured Arc/Arg3.1 level in the hippocampus. Arc/Arg3.1 expression was significantly decreased 1 h after administration of baclofen (Fig. 4*G*). Together these results indicated that elevated levels of $GABA_B$R activity in S783A mice reduced the downstream activity and expression levels of proteins that are critical for memory formation.

S783A mice exhibited enhanced AMPAR surface expression and synaptic density

Arc/Arg3.1 is believed to play a critical role in cognition in part by its ability to promote AMPAR endocytosis. Consistent with this, Arc/Arg3.1-deficient mice have increased levels of AMPAR expression and increased density of mushroom spines in the CA1 region of the hippocampus (Chowdhury et al., 2006; Plath et al., 2006; Peebles et al., 2010). In agreement with these studies, the surface expression levels of the AMPAR subunits GluA1 and GluA2 were significantly increased in the hippocampal slices from S783A mice ($p < 0.01$; Fig. 5*A*,*B*). We also performed electrophysiological analysis to compare AMPAR function between genotypes. A robust increase in the density of glutamate-activated currents was evident in S783A compared with WT mice ($p < 0.05$; Fig. 5*C*,*D*).

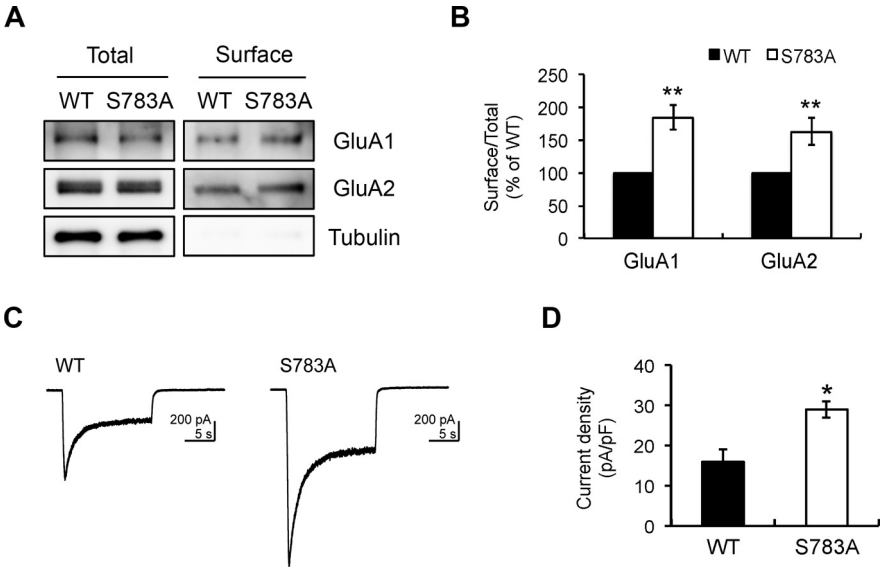

Figure 5. Increased AMPAR surface expression in S783A mice. ***A***, ***B***, Increased surface expression of AMPARs in S783A mice. Hippocampal slices prepared from WT and S783A mice were used for steady-stated biotinylation of surface GluA1 and GluA2 subunits. ***A***, Total GluA1 and GluA2 subunits are shown to the left, and the biotinylated surface GluA1 and GluA2 subunits are shown to the right. Tubulin was used as a control. ***B***, Quantification of surface AMPAR levels (ratio of surface to total) in WT and S783A mice. Data are normalized to WT and represented mean ± SEM. $n = 4–5$, $^{**}p < 0.01$; Student's *t* test. ***C***, Representative traces of glutamate-activated currents from WT and S783A hippocampal neurons. ***D***, Graph depicts the average glutamate current density values of WT and S783A neurons, data represent mean ± SEM (WT, $n = 3$; S783A, $n = 4$, $^{*}p < 0.05$, unpaired *t* test).

We then compared synapse number and structure in CA1 stratum radiatum using electron microscopy (Fig. 6*A–E*). The total number of excitatory synapses was significantly increased in S783A mice (Fig. 6*A*,*C*). Surprisingly, the length of PSDs in CA1 excitatory synapses was larger in S783A mice compared with WT controls (Fig. 6*B*,*D*,*E*). Consistent with the above, the expression of PSD-95 was enhanced in S783A mice, but not the synaptic vesicle protein synaptophysin or synaptic marker synapsin I (Fig. 6*F–I*). These data strongly suggested that the enhanced postsynaptic $GABA_BR$ activity in S783A mice led to a pronounced modification in the architecture of excitatory synapses.

S783A exhibited impaired long-term spatial memory

Our results suggest that potentiation in the activity of postsynaptic $GABA_BRs$ results in deficits in Arc/Arg3.1 expression and profound alterations in neuronal morphology. Therefore we performed behavioral analyses to compare specific aspects of cognition in S783A and WT mice. We first examined contextual and cued memory 24 h after fear conditioning. The S783A mice showed a significant deficit in hippocampal contextual fear, as evidenced by reduced freezing behavior (Fig. 7*A*,*B*), but not in auditory cued behavior (Fig. 7*A*). Deficits in contextual fear memory are correlated with decreased hippocampal-dependent spatial memory (Bach et al., 1995). We then examined object recognition to further evaluate the role of the S783A mutation in memory formation (Ennaceur and Delacour, 1988). After habituation to the context, mice were exposed to an identical pair of objects for 10 min (training period) and, 24 h later, a 5 min test was conducted in which mice were allowed to explore the previously exposed (familiar) object and a novel object (Fig. 7*C*). Both groups of mice demonstrated greater exploration of the novel object over the familiar object (Fig. 7*D*,*E*). We also examined S738A mice in the spatial object recognition task (Haettig et al., 2011). In this version, all animals were exposed to two identical objects for 10 min and, 24 h later, one of the objects was moved to a novel position (Fig. 7*F*). During the training sessions, both genotypes spent the same amount of time exploring the two identical objects ($p = 0.8241$). However S783A mice failed to distinguish between the object that remained in place and the object that was moved. Their WT counterparts, meanwhile, preferentially investigated the displaced object (Fig. 7*G*,*H*). These behavioral tests suggested that S783A mice have selective deficits in long-term spatial memory.

To further assess spatial learning and memory, we used the Barnes maze (Barnes, 1979) over a training period of 4 d (two trials per day). WT mice improved performance over 4 d, as indicated by a progressive reduction in total latency to enter into the target hole ($p < 0.0001$) and in total errors ($p < 0.01$) across trials. In contrast, S783A mice showed a significant decrease in total latency ($p < 0.0001$) but did not exhibit improvements in total errors ($p = 0.5517$; Fig. 8*A*,*B*). We corroborated our findings by analyzing primary parameters. Spatial learning in S783A mice was evident by a significant reduction in the primary latency ($p < 0.0001$; Fig. 8*C*) but no improvements were observed in primary errors ($p = 0.0784$; Fig. 8*D*), indicating that S783A mice reached the target hole with reduced latency just as WT mice did but persisted in choosing a wrong hole before reaching the target hole. After the 4 d training period, we performed a probe trial to test memory retention on day 5 (1 d after the last day of training) and day 12. On day 5, no difference was observed in the primary latency (Fig. 8*E*), primary error (Fig. 8*F*), and distance traveled (Fig. 8*G*) between genotypes. However S783A mice showed a statistically significant difference in all three parameters between days 5 and 12 ($p < 0.05$), indicating that S783A mice have reduced memory retention compared with WT (Fig. 8*E–G*). Collectively, these behavioral tests independently confirmed that S783A mice exhibited impaired long-term spatial memory. Importantly, S783A mice showed normal performance in batteries of home cage activity (Fig. 9*A*) and anxiety-like behavior (Fig. 9*B*,*C*). Together, our study clearly demonstrated that the efficacy of postsynaptic $GABA_BR$ signaling is a critical determinant of spatial memory consolidation.

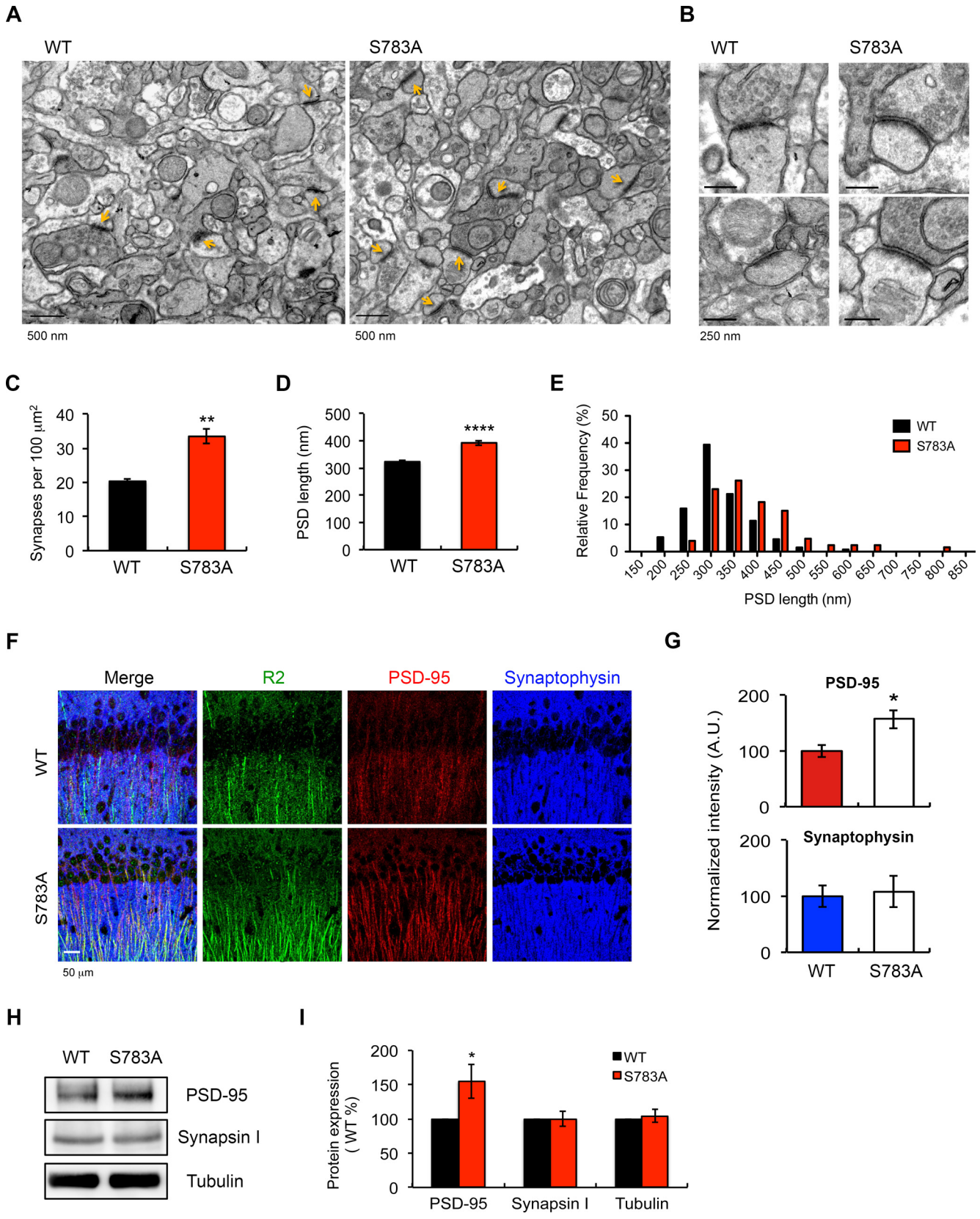

Figure 6. Synapse density and PSD-95 expression are increased in S783A mice. ***A***, Electron microscopy images of CA1 stratum radiatum region in WT and S783A mice. Representative excitatory synapses are indicated (yellow arrow). Scale bars, 500 nm. ***B***, Micrograph showing an asymmetric excitatory synapse identified by electron-dense PSD. Scale bars, 250 nm. ***C***, Synapse density expressed as mean ± SEM per 100 μm^2 in CA1 stratum radiatum region. $^{**}p < 0.01$; unpaired *t* test. ***D***, Mean PSD length determined by analyses of electron microscopy images. Shown are mean ± SEM from four WT and three S783A mice. $n = 180–200$ per genotype; $^{****}p < 0.0001$; unpaired *t* test. ***E***, Histogram of frequency distribution of PSD length observed in electron microscopy analysis from WT and S783A mice, analyzed as in ***D***. ***F***, ***G***, Expression of synaptic markers in CA1 region of hippocampus. ***F***, Representative confocal images of $GABA_BR2$ subunit (green), PSD-95 (red), and synaptophysin (blue) in WT and S783A mice. ***G***, Normalized quantification of PSD-95 and synaptophysin expression in CA1 region of hippocampus. (*Figure legend continues*.)

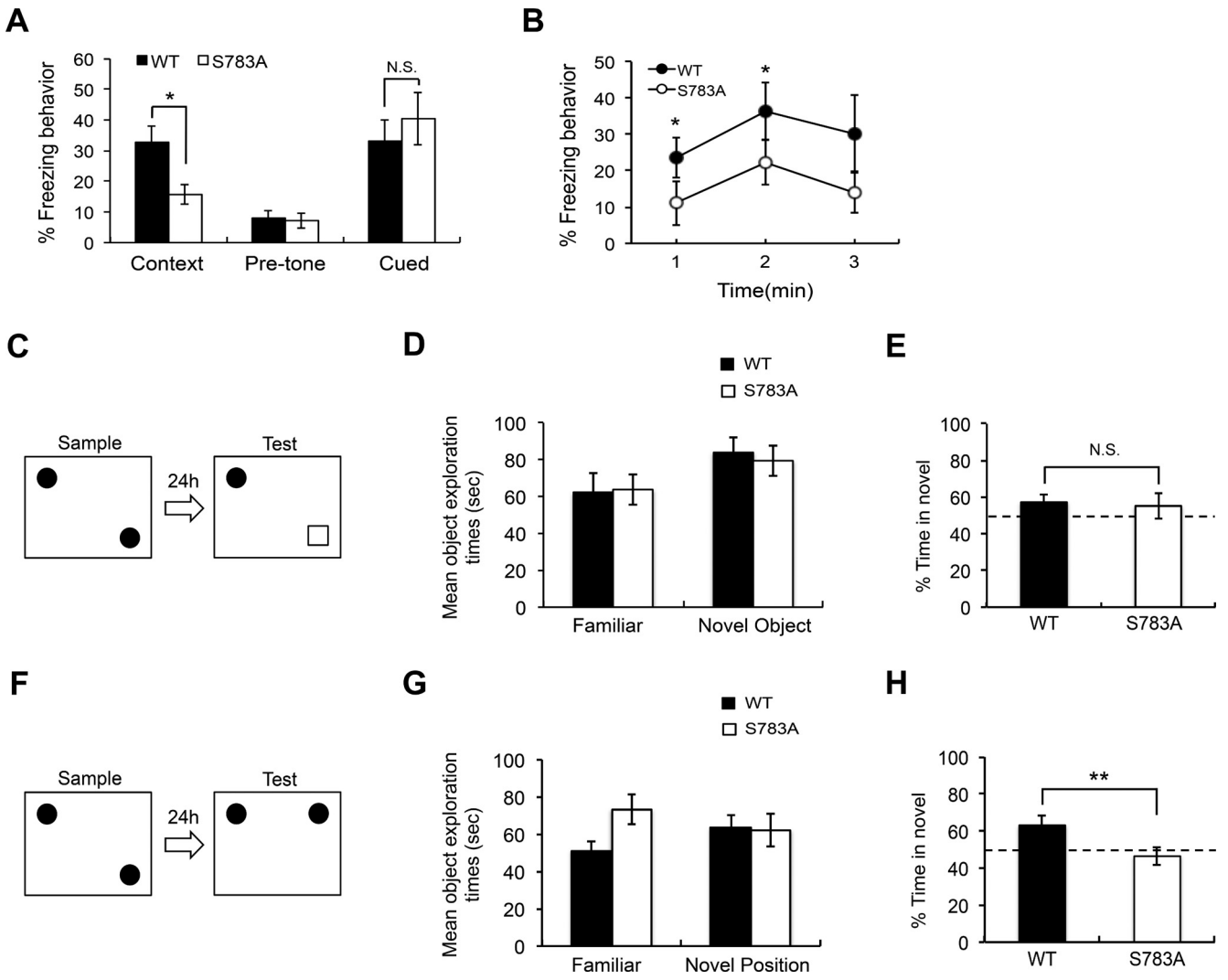

Figure 7. Disrupted spatial memory consolidation during fear conditioning and object recognition. ***A***, ***B***, Contextual and cued fear-conditioning test. ***A***, Average of conditioned freezing during contextual and cued test. Percentage of time freezing during the conditioned context (Context), before conditioning (Pre-tone), and during the tone presentation (Cued) is shown ($n = 11$ each). $p = 0.369$; two-tailed t test. ***B***, Percentage time freezing during the 3 min of the conditioned context without foot-shock stimulus ($n = 11$ each). S783A mice spent significantly less time freezing than did WT mice. $^*p < 0.05$; one-way ANOVA. ***C–E***, Novel-object recognition test. ***C***, Diagram of the object recognition task. ***D***, Novel-object recognition 24 h after acquisition. The graph shows the object exploration during the 5 min test phase of the object recognition task ($n = 10$ each). ***E***, The times spent exploring a novel object is shown as a ratio of the total time spent exploring both objects. Both WT and S783A mice spent more time exploring a novel object ($p > 0.05$, 2-tailed t test). ***F–H,*** Spatial object recognition test. ***F***, Diagram of the spatial object recognition task. ***G***, Spatial object recognition 24 h after acquisition. The graph shows the object exploration during the 5 min test phase of the object recognition task ($n = 10$ each). ***H***, The times spent exploring object in a novel position is shown as a ratio of the total time spent exploring both objects. S783A mice did not display any preference for an object placed to a novel position (WT, 63.11 ± 5.0%; S783A, 46.46 ± 4.75%, $^*p < 0.05$, 2-tailed t test). All data represent mean ± SEM.

S783A mice exhibited enhanced synaptic plasticity

S783A mice exhibited deficits in long-term spatial memory and activation of Arc/Arg3.1 expression. We therefore tested whether S783A mice have altered hippocampal LTP. We used two different protocols for LTP induction: two theta-burst stimulation (2 TBS; four pulses at 100 Hz with an interburst interval of 0.2 s) and five theta-burst stimulation (5 TBS). Two TBS increased the magnitude of LTP in S783A mice immediately after induction compared with WT (S783A, 3.96 ± 0.389 of baseline; WT, 2.109 ± 0.289 of baseline; Fig. 10*A*) and remained significantly larger 50 min after induction (S783A, 1.87 ± 0.16 of baseline; WT, 1.4 ± 0.05 of baseline; $p < 0.05$; Fig. 10*A*). Interestingly, LTP induced by the 5 TBS protocol was similar in S783A and WT mice (S783A, 2.34 ± 0.089 of baseline at 50 min postinduction; WT, 2.09 ± 0.165 of baseline at 50 min postinduction, $p = 0.21$; Fig. 10*B*). Importantly, when we compared the magnitude of LTP between the 2 TBS and 5 TBS protocol, S783A slices showed only a small increase in 5 TBS compared with 2 TBS; however, in WT slices, 5 TBS largely increased the levels of LTP (Fig. 10*A*,*B*). These results suggested that 2 TBS saturated the levels of LTP in S783A mice but not in WT, which is likely to reflect the higher number of AMPARs in the mutant mouse. Together our results strongly demonstrated that the enhanced activity of postsynaptic $GABA_B$Rs leads to changes in key proteins that

←

(*Figure legend continued.*) Shown are mean ± SEM from five independent experiments. $^*p < 0.05$; Student's t test. ***H***, Western blot analysis of hippocampus dissected from WT and S783A mice. Immunoblots were probed with antibodies for PSD-95, synapsin I, and tubulin. ***I***, Quantification of PSD-95 and synapsin I in hippocampi of S783A mice (ratio to tubulin). Data are shown as a change relative to WT and represent mean ± SEM. $n = 6$; $^*p < 0.05$; Student's t test.

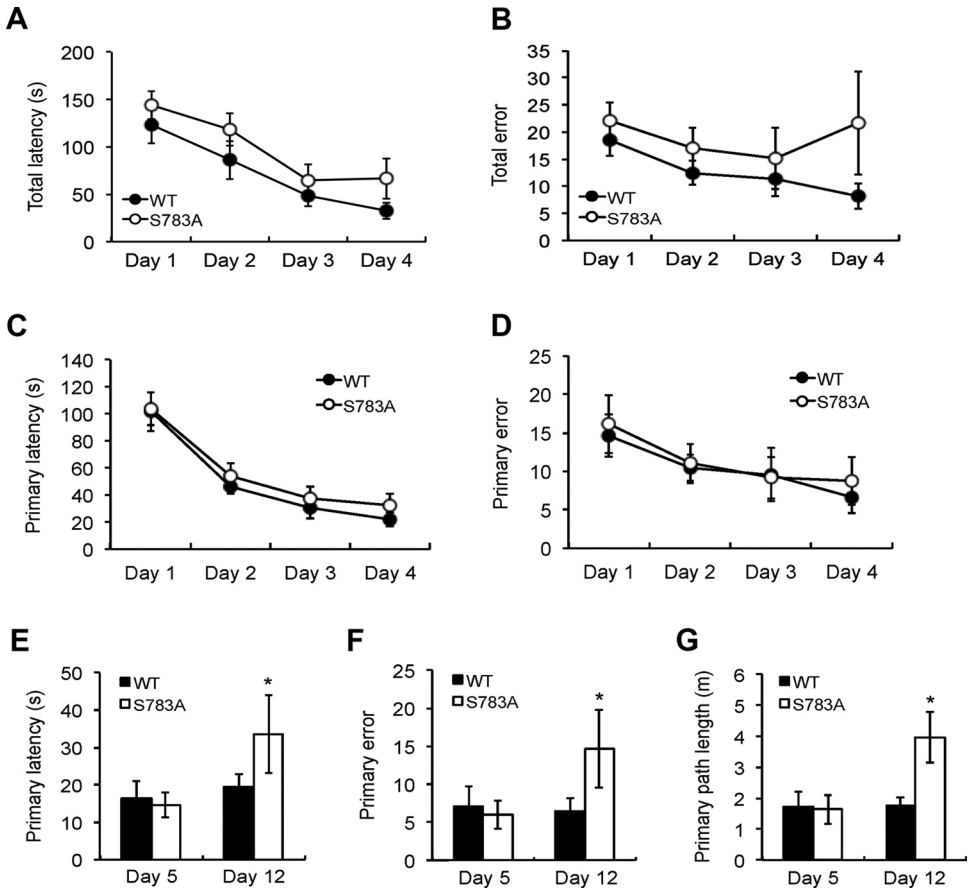

Figure 8. Impaired spatial memory consolidation in the Barnes maze in S783A mice. ***A***, ***B***, Results of WT and S783A mice subjected to Barnes maze test during 4 d of training. ***A***, Total latency (in seconds) by trials (days) to find the target hole. Both WT and S783A mice improved to find a target ($p < 0.0001$, repeated-measurements ANOVA, $n = 10$). No difference was found between genotypes ($p = 0.8142$, 2-way ANOVA). ***B***, Total error by trials. Only WT showed significant improvement in total error (WT, $p < 0.01$; S783A, $p = 0.5517$, repeated-measurements ANOVA, $n = 10$). No difference was found between genotypes ($p = 0.3264$, 2-way ANOVA). ***C***, Primary latency (in seconds) by trials (days) to find the target hole. Both WT and S783A mice improved to find a target ($p < 0.0001$, repeated-measurements ANOVA. $n = 10$). No difference was found between genotypes ($p = 0.9746$, 2-way ANOVA). ***D***, Primary error by trials. WT mice, but not S783A mice, showed significant improvement in primary error (WT, $p < 0.05$; S783A, $p = 0.0784$, repeated-measurements ANOVA, $n = 10$). All data represent mean ± SEM. ***E–G***, Probe trial for memory retention test. ***E***, Primary latency (in seconds). S783A mice spent more time searching target hole (day 5 vs 12: WT, $p = 0.3048$; S783A, $^*p < 0.05$, paired Student's *t* test). ***F***, Primary error. S783A mice made more errors in attempting to reach to the target hole (day 5 vs 12: WT, $p = 0.4244$; S783A, $^*p < 0.05$, paired Student's *t* test). ***G***, Primary path length (in meters) traveled. S783A mice showed an increase in primary path length (day 5 vs 12: WT, $p = 0.323$; S783A, $^*p < 0.05$, paired Student's *t* test). All data represent mean ± SEM.

mediate excitatory synaptic transmission and alter synaptic plasticity.

Discussion

Our work demonstrated for the first time a direct connection between the postsynaptic $GABA_BR$ activity and long-term spatial memory. Using mice in which the $GABA_BR$ subunit degradation had been abolished by mutation (S783A mice), we revealed a key role for $GABA_BR$ activity in regulating the molecular mechanisms that underlie specific aspects of memory formation.

Studies in expression systems and cultured neurons have established that phosphorylation and dephosphorylation of $GABA_BRs$ regulate their activity and trafficking (Terunuma et al., 2010a,b). Phosphorylation of S783 in the $GABA_BR2$ subunit by AMPK increases coupling to GIRKs, but also prevents receptor internalization and lysozomal degradation (Kuramoto et al., 2007; Terunuma et al., 2010b), effects that can be mimicked by mutation to alanine residues. Meanwhile, the S783A mutants are stable on the cell surface and $GABA_BR$-mediated GIRK rundown is abraded (Kuramoto et al., 2007; Terunuma et al., 2010b). We therefore created S783A mice to begin to assess the physiological significance of $GABA_BR$ phosphorylation. S783A mice had higher cell-surface expression levels of the $GABA_BR1b/R2$ heterodimer, which is consistent with the role of this residue in stabilizing surface receptors and limiting endocytosis and subsequent lysozomal degradation (Terunuma et al., 2010b). Our functional assays determined that there were no differences in excitatory presynaptic $GABA_BR$ activity. By contrast, postsynaptic $GABA_BR$ activity was significantly enhanced in S783A mice as measured by their ability to activate GIRKs. The selective effect of the S783A mutation on postsynaptic $GABA_BR$ activity indicates that presynaptic receptors are very stable and do not exhibit significant rates of endocytosis, whereas their postsynaptic counterparts show higher rates of phospho-dependent internalization (Vargas et al., 2008; Terunuma et al., 2010b). It is possible that this selective effect is due to low AMPK and PP2A activity in presynaptic terminals of the hippocampal neurons or to differential binding complexes of presynaptic versus postsynaptic $GABA_BRs$.

Given the enhanced $GABA_BR$ activity in S783A mice, we examined Arc/Arg3.1 expression. Arc/Arg3.1 expression is regulated by neural activity and is a key regulator of long-term memory formation (Bourtchuladze et al., 1994; Guzowski et al.,

2000; Athos et al., 2002; Plath et al., 2006). Total Arc/Arg3.1 expression levels were significantly reduced in S783A mice. Furthermore, treatment with the highly potent and selective $GABA_BR$ antagonist CGP54626 restored Arc/Arg3.1 expression levels in S783A mice while activation of $GABA_BRs$ in WT mice dramatically reduced Arc/Arg3.1 expression. It is therefore possible that the enhancement of cognitive performance by $GABA_BR$ antagonists and the suppression of working memory by agonists in rodents and monkeys may be due to the modulation of Arc/Arg3.1 expression through $GABA_BRs$ (Mondadori et al., 1993; DeSousa et al., 1994; Froestl et al., 2004).

It has been reported that Arc/Arg3.1 knock-out mice express high levels of surface AMPARs due to blockade of endocytosis (Chowdhury et al., 2006; Shepherd et al., 2006). Furthermore, Arc/Arg3.1 knock-out neurons exhibit increased spine width in AMPAR-containing spines (Peebles et al., 2010; Okuno et al., 2012). These observations are similar to our electrophysiological and biochemical analyses, which revealed increased levels of AMPARs, density of excitatory synapses, and PSD length in S783A mice. Consistent with an increase in the density of excitatory synapses, PSD-95 expression was significantly elevated in S783A mice. Given the increase in $GABA_BR$ activity in S783A mice, this increase in excitatory synapse number and PSD length may reflect an adaptive compensatory mechanism to maintain excitatory–inhibitory balance, since we did not observe changes in basal synaptic transmission. Alternatively, the effects of the S783A mutation on excitatory synapses could be a direct consequence of enhancing $GABA_BR$-mediated downregulation of Arc/Arg3.1 expression, which in turn elevated AMPAR surface expression. Indeed, PSD-95 overexpression increases AMPAR clustering and enhances the size and number of spines (El-Husseini et al., 2000) and AMPAR overexpression in cultured neurons increases the length and number of excitatory synapses (Chen et al., 2009). It is possible that the dysregulated accumulation of AMPARs at the surface of spines in S783A mice caused the increase of PSD-95. However, we did not detect differences in basic synaptic transmission and evoked EPSCs in S783A mice, but we did observe larger glutamate-activated whole-cell currents, which indicate that the additional AMPARs only become activated under specific conditions. Supporting this observation, we found LTP induced by the 2 TBS protocol was higher in S783A mice compared with WT mice but not in the 5 TBS protocol. It is still possible that the additional AMPARs are preferentially targeted to or form silent synapses (Okuno et al., 2012). This rationale implies that $GABA_BR$ signaling directly influences the levels of both excitation and inhibition. Significantly, enhanced LTP and loss of spatial memory seen in S783A mice has been previously reported in several genetically altered mice, including PSD-95 mutant mice (Migaud et al., 1998), CaMKK α knock-out mice (Blaeser et al., 2006), and Arc/Arg3.1 knock-out mice (Plath et al., 2006).

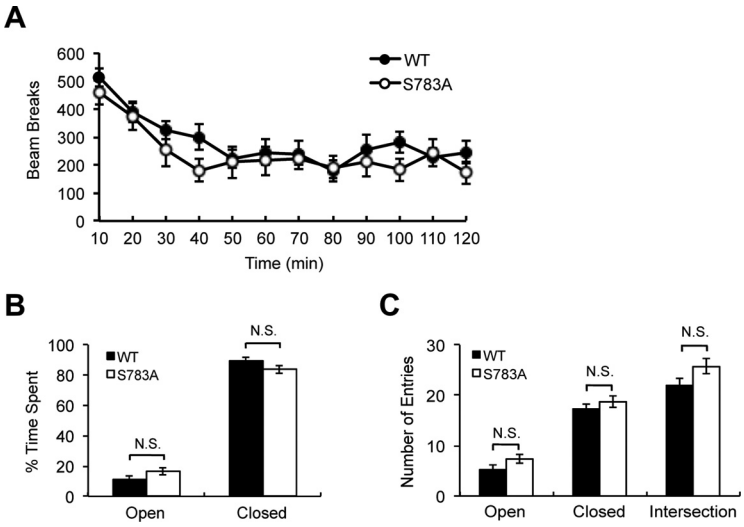

Figure 9. Behavioral tests in S783A mice. ***A***, Home cage activity test. Normal behavioral activity in S783A mice. Shown is number of beam breaks per 10 min. $n = 10$, $p = 0.2253$, unpaired *t* test. All data represent mean ± SEM. ***B–C***, Elevated plus maze test. Anxiety-like behavior does not differ between WT and S783A mice as measured by the time spent in the open and closed arms divided by the time in all arms (***B***, unpaired *t* test: open arms, $p = 0.1774$; closed arms, $p = 0.1773$), or as measured by the number of entries into each arm (***C***, unpaired *t* test: open arms, $p = 0.105$, closed arms, $p = 0.3905$; intersection, $p = 0.094$). $n = 11$ littermate pairs. All data represent the mean ± SEM.

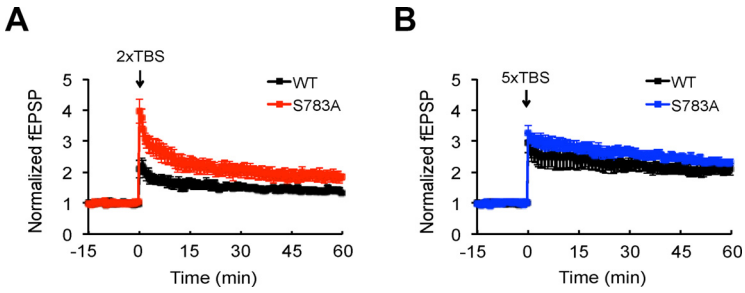

Figure 10. Enhanced hippocampal LTP with impaired $GABA_BR$ phosphorylation in S783A mice. ***A***, LTP induced by 2 TBS at the CA1 pyramidal neuron was shown. Average normalized (against baseline) fEPSP rise slope in the WT (black) and S783A (red) slices. Error bars represent ± SEM from four independent experiments. Two-tailed *t* test. ***B***, LTP induced by 5 TBS decayed more slowly than the potentiation elicited by 2 TBS. There was no significant difference between the mean fEPSP slopes measured in WT and S783A mice 50 min after stimulation. Error bars represent ± SEM from four independent experiments. $p = 0.21$, two-tailed *t* test.

Our behavioral characterization of S783A mice revealed no difference in basal activity or anxiety-like behaviors. However, these mice exhibited a deficit in contextual fear memory, which is associated with hippocampal-dependent spatial memory (Bach et al., 1995). Furthermore, the probe test using the Barnes maze demonstrated that S783A mice exhibited impaired memory retention, which is also connected with hippocampal function (Barnes, 1979). These results match what has been observed in Arc/Arg3.1 knock-out mice, which express enhanced surface AMPAR levels but are impaired in long-term spatial memory (Plath et al., 2006). It is noteworthy that S783A mice were able to learn during the training periods of tasks designed to test spatial memory and our results did not rule out the possibility of impairment in hippocampal-independent forms of long-term memory.

Collectively, our study demonstrated an unacknowledged postsynaptic mechanism by which $GABA_BRs$ regulate long-term spatial memory. Mutation of S783 had numerous consequences on the downstream targets. These consequences were ultimately

manifested as deficits in long-term spatial memory and memory consolidation. These results highlight the potential role of compounds that alter $GABA_BR$ signaling to enhance cognitive function.

References

Athos J, Impey S, Pineda VV, Chen X, Storm DR (2002) Hippocampal CRE-mediated gene expression is required for contextual memory formation. Nat Neurosci 5:1119–1120. CrossRef Medline

Bach ME, Hawkins RD, Osman M, Kandel ER, Mayford M (1995) Impairment of spatial but not contextual memory in CaMKII mutant mice with a selective loss of hippocampal LTP in the range of the theta frequency. Cell 81:905–915. CrossRef Medline

Barnes CA (1979) Memory deficits associated with senescence: a neurophysiological and behavioral study in the rat. J Comp Physiol Psychol 93:74–104. CrossRef Medline

Bettler B, Tiao JY (2006) Molecular diversity, trafficking and subcellular localization of GABAB receptors. Pharmacol Ther 110:533–543. CrossRef Medline

Blaeser F, Sanders MJ, Truong N, Ko S, Wu LJ, Wozniak DF, Fanselow MS, Zhuo M, Chatila TA (2006) Long-term memory deficits in Pavlovian fear conditioning in Ca2+/calmodulin kinase kinase alpha-deficient mice. Mol Cell Biol 26:9105–9115. CrossRef Medline

Bloomer WA, VanDongen HM, VanDongen AM (2008) Arc/Arg3.1 translation is controlled by convergent N-methyl-D-aspartate and Gs-coupled receptor signaling pathways. J Biol Chem 283:582–592. Medline

Bourtchuladze R, Frenguelli B, Blendy J, Cioffi D, Schutz G, Silva AJ (1994) Deficient long-term memory in mice with a targeted mutation of the cAMP-responsive element-binding protein. Cell 79:59–68. CrossRef Medline

Bowery NG, Bettler B, Froestl W, Gallagher JP, Marshall F, Raiteri M, Bonner TI, Enna SJ (2002) International Union of Pharmacology. XXXIII. Mammalian gamma-aminobutyric acid(B) receptors: structure and function. Pharmacol Rev 54:247–264. CrossRef Medline

Brucato FH, Levin ED, Mott DD, Lewis DV, Wilson WA, Swartzwelder HS (1996) Hippocampal long-term potentiation and spatial learning in the rat: effects of $GABA_B$ receptor blockade. Neuroscience 74:331–339. CrossRef Medline

Chen W, Prithviraj R, Mahnke AH, McGloin KE, Tan JW, Gooch AK, Inglis FM (2009) AMPA glutamate receptor subunits 1 and 2 regulate dendrite complexity and spine motility in neurons of the developing neocortex. Neuroscience 159:172–182. CrossRef Medline

Chowdhury S, Shepherd JD, Okuno H, Lyford G, Petralia RS, Plath N, Kuhl D, Huganir RL, Worley PF (2006) Arc/Arg3.1 interacts with the endocytic machinery to regulate AMPA receptor trafficking. Neuron 52:445–459. CrossRef Medline

Couve A, Moss SJ, Pangalos MN (2000) $GABA_B$ receptors: a new paradigm in G protein signaling. Mol Cell Neurosci 16:296–312. CrossRef Medline

Couve A, Thomas P, Calver AR, Hirst WD, Pangalos MN, Walsh FS, Smart TG, Moss SJ (2002) Cyclic AMP-dependent protein kinase phosphorylation facilitates GABA(B) receptor-effector coupling. Nat Neurosci 5:415–424. Medline

Deng Q, Terunuma M, Fellin T, Moss SJ, Haydon PG (2011) Astrocytic activation of A1 receptors regulates the surface expression of NMDA receptors through a Src kinase dependent pathway. Glia 59:1084–1093. CrossRef Medline

DeSousa NJ, Beninger RJ, Jhamandas K, Boegman RJ (1994) Stimulation of $GABA_B$ receptors in the basal forebrain selectively impairs working memory of rats in the double Y-maze. Brain Res 641:29–38. CrossRef Medline

El-Husseini AE, Schnell E, Chetkovich DM, Nicoll RA, Bredt DS (2000) PSD-95 involvement in maturation of excitatory synapses. Science 290:1364–1368. Medline

Ennaceur A, Delacour J (1988) A new one-trial test for neurobiological studies of memory in rats. 1: behavioral data. Behav Brain Res 31:47–59. CrossRef Medline

Froestl W, Gallagher M, Jenkins H, Madrid A, Melcher T, Teichman S, Mondadori CG, Pearlman R (2004) SGS742: the first GABA(B) receptor antagonist in clinical trials. Biochem Pharmacol 68:1479–1487. CrossRef Medline

Gu J, Lee CW, Fan Y, Komlos D, Tang X, Sun C, Yu K, Hartzell HC, Chen G, Bamburg JR, Zheng JQ (2010) ADF/cofilin-mediated actin dynamics regulate AMPA receptor trafficking during synaptic plasticity. Nat Neurosci 13:1208–1215. CrossRef Medline

Guzowski JF, Lyford GL, Stevenson GD, Houston FP, McGaugh JL, Worley PF, Barnes CA (2000) Inhibition of activity-dependent arc protein expression in the rat hippocampus impairs the maintenance of long-term potentiation and the consolidation of long-term memory. J Neurosci 20:3993–4001. Medline

Haettig J, Stefanko DP, Multani ML, Figueroa DX, McQuown SC, Wood MA (2011) HDAC inhibition modulates hippocampus-dependent long-term memory for object location in a CBP-dependent manner. Learn Mem 18:71–79. CrossRef Medline

Kaupmann K, Huggel K, Heid J, Flor PJ, Bischoff S, Mickel SJ, McMaster G, Angst C, Bittiger H, Froestl W, Bettler B (1997) Expression cloning of GABA(B) receptors uncovers similarity to metabotropic glutamate receptors. Nature 386:239–246. CrossRef Medline

Kuramoto N, Wilkins ME, Fairfax BP, Revilla-Sanchez R, Terunuma M, Tamaki K, Iemata M, Warren N, Couve A, Calver A, Horvath Z, Freeman K, Carling D, Huang L, Gonzales C, Cooper E, Smart TG, Pangalos MN, Moss SJ (2007) Phospho-dependent functional modulation of GABA(B) receptors by the metabolic sensor AMP-dependent protein kinase. Neuron 53:233–247. CrossRef Medline

Link W, Konietzko U, Kauselmann G, Krug M, Schwanke B, Frey U, Kuhl D (1995) Somatodendritic expression of an immediate early gene is regulated by synaptic activity. Proc Natl Acad Sci U S A 92:5734–5738. CrossRef Medline

Migaud M, Charlesworth P, Dempster M, Webster LC, Watabe AM, Makhinson M, He Y, Ramsay MF, Morris RG, Morrison JH, O'Dell TJ, Grant SG (1998) Enhanced long-term potentiation and impaired learning in mice with mutant postsynaptic density-95 protein. Nature 396:433–439. CrossRef Medline

Mondadori C, Jaekel J, Preiswerk G (1993) CGP 36742: the first orally active $GABA_B$ blocker improves the cognitive performance of mice, rats, and rhesus monkeys. Behav Neural Biol 60:62–68. CrossRef Medline

Mondadori C, Möbius HJ, Borkowski J (1996) The $GABA_B$ receptor antagonist CGP 36,742 and the nootropic oxiracetam facilitate the formation of long-term memory. Behav Brain Res 77:223–225. CrossRef Medline

Mott DD, Lewis DV (1994) The pharmacology and function of central $GABA_B$ receptors. Int Rev Neurobiol 36:97–223. Medline

Okuno H, Akashi K, Ishii Y, Yagishita-Kyo N, Suzuki K, Nonaka M, Kawashima T, Fujii H, Takemoto-Kimura S, Abe M, Natsume R, Chowdhury S, Sakimura K, Worley PF, Bito H (2012) Inverse synaptic tagging of inactive synapses via dynamic interaction of Arc/Arg3.1 with CaMKII-beta. Cell 149:886–898. CrossRef Medline

Peebles CL, Yoo J, Thwin MT, Palop JJ, Noebels JL, Finkbeiner S (2010) Arc regulates spine morphology and maintains network stability *in vivo*. Proc Natl Acad Sci U S A 107:18173–18178. CrossRef Medline

Plath N, Ohana O, Dammermann B, Errington ML, Schmitz D, Gross C, Mao X, Engelsberg A, Mahlke C, Welzl H, Kobalz U, Stawrakakis A, Fernandez E, Waltereit R, Bick-Sander A, Therstappen E, Cooke SF, Blanquet V, Wurst W, Salmen B, et al. (2006) Arc/Arg3.1 is essential for the consolidation of synaptic plasticity and memories. Neuron 52:437–444. CrossRef Medline

Rust MB, Gurniak CB, Renner M, Vara H, Morando L, Görlich A, Sassoè-Pognetto M, Banchaabouchi MA, Giustetto M, Triller A, Choquet D, Witke W (2010) Learning, AMPA receptor mobility and synaptic plasticity depend on n-cofilin-mediated actin dynamics. EMBO J 29:1889–1902. CrossRef Medline

Satoh Y, Endo S, Ikeda T, Yamada K, Ito M, Kuroki M, Hiramoto T, Imamura O, Kobayashi Y, Watanabe Y, Itohara S, Takishima K (2007) Extracellular signal-regulated kinase 2 (ERK2) knockdown mice show deficits in long-term memory; ERK2 has a specific function in learning and memory. J Neurosci 27:10765–10776. CrossRef Medline

Schuler V, Lüscher C, Blanchet C, Klix N, Sansig G, Klebs K, Schmutz M, Heid J, Gentry C, Urban L, Fox A, Spooren W, Jaton AL, Vigouret J, Pozza M, Kelly PH, Mosbacher J, Froestl W, Käslin E, Korn R, et al. (2001) Epilepsy, hyperalgesia, impaired memory, and loss of pre- and postsynaptic GABA(B) responses in mice lacking GABA(B(1)). Neuron 31:47–58. CrossRef Medline

Shepherd JD, Rumbaugh G, Wu J, Chowdhury S, Plath N, Kuhl D, Huganir RL, Worley PF (2006) Arc/Arg3.1 mediates homeostatic synaptic scaling of AMPA receptors. Neuron 52:475–484. CrossRef Medline

Takahashi T, Kajikawa Y, Tsujimoto T (1998) G-protein-coupled modula-

tion of presynaptic calcium currents and transmitter release by a $GABA_B$ receptor. J Neurosci 18:3138–3146. Medline

Terunuma M, Jang IS, Ha SH, Kittler JT, Kanematsu T, Jovanovic JN, Nakayama KI, Akaike N, Ryu SH, Moss SJ, Hirata M (2004) $GABA_A$ receptor phospho-dependent modulation is regulated by phospholipase C-related inactive protein type 1, a novel protein phosphatase 1 anchoring protein. J Neurosci 24:7074–7084. CrossRef Medline

Terunuma M, Xu J, Vithlani M, Sieghart W, Kittler J, Pangalos M, Haydon PG, Coulter DA, Moss SJ (2008) Deficits in phosphorylation of GABA(A) receptors by intimately associated protein kinase C activity underlie compromised synaptic inhibition during status epilepticus. J Neurosci 28:376–384. CrossRef Medline

Terunuma M, Pangalos MN, Moss SJ (2010a) Functional modulation of $GABA_B$ receptors by protein kinases and receptor trafficking. Adv Pharmacol 58:113–122. Medline

Terunuma M, Vargas KJ, Wilkins ME, Ramírez OA, Jaureguiberry-Bravo M, Pangalos MN, Smart TG, Moss SJ, Couve A (2010b) Prolonged activation of NMDA receptors promotes dephosphorylation and alters postendocytic sorting of $GABA_B$ receptors. Proc Natl Acad Sci U S A 107:13918–13923. CrossRef Medline

Tretter V, Revilla-Sanchez R, Houston C, Terunuma M, Havekes R, Florian C, Jurd R, Vithlani M, Michels G, Couve A, Sieghart W, Brandon N, Abel T, Smart TG, Moss SJ (2009) Deficits in spatial memory correlate with modified {gamma}-aminobutyric acid type A receptor tyrosine phosphorylation in the hippocampus. Proc Natl Acad Sci U S A 106:20039–20044. CrossRef Medline

Vargas KJ, Terunuma M, Tello JA, Pangalos MN, Moss SJ, Couve A (2008) The availability of surface GABA B receptors is independent of gamma-aminobutyric acid but controlled by glutamate in central neurons. J Biol Chem 283:24641–24648. CrossRef Medline

Vigot R, Barbieri S, Bräuner-Osborne H, Turecek R, Shigemoto R, Zhang YP, Luján R, Jacobson LH, Biermann B, Fritschy JM, Vacher CM, Müller M, Sansig G, Guetg N, Cryan JF, Kaupmann K, Gassmann M, Oertner TG, Bettler B (2006) Differential compartmentalization and distinct functions of $GABA_B$ receptor variants. Neuron 50:589–601. CrossRef Medline

Waung MW, Pfeiffer BE, Nosyreva ED, Ronesi JA, Huber KM (2008) Rapid translation of Arc/Arg3.1 selectively mediates mGluR-dependent LTD through persistent increases in AMPAR endocytosis rate. Neuron 59:84–97. CrossRef Medline